materials

MDPI

Article

Acid-Induced Mechanical Degradation and Microstructural Damage of Shield Muck Solidified with ESCA and P.O 42.5 Cement

Liandi Zhao [1], Long Ma [1,*], Jie Li [2], Fengming Chu [2], Henggen Zhang [1,3,*], Shen Zuo [1], Jin Li [1], Junwei Bi [1,4], Biao Geng [5] and Feiyan Jin [6]

[1] Shandong Key Laboratory of Technologies and Systems for Intelligent Construction Equipment, Shandong Jiaotong University, Jinan 250357, China
[2] Tai'an Xiaoran Landscape and Municipal Engineering Co., Ltd., Tai'an 271000, China
[3] Shandong Engineering Research Center of Marine Exploration and Conservation, Ocean University of China, Qingdao 266100, China
[4] School of Qilu Transportation, Shandong University, Jinan 250002, China
[5] Intelligent Transportation, Shandong Jiaotong University, Jinan 250357, China
[6] College of Environmental and Resource Sciences, Zhejiang University, Hangzhou 310058, China
* Correspondence: 16678333521@163.com (L.M.); 250058@sdjtu.edu.cn (H.Z.)

Abstract

To elucidate the mechanical degradation and microstructural damage of solidified shield muck under acid attack, an early-strength composite cementitious agent (ESCA) and P.O 42.5 ordinary Portland cement were used as solidifying binders, followed by 45-day immersion tests at pH values of 1, 3, 5, and 7. The evolution of macroscopic properties and microstructure of the two solidification systems was evaluated through measurements of mass and P-wave velocity, stress–strain response, failure characteristics, scanning electron microscopy (SEM), and industrial computed tomography (CT). The results showed that the physical and mechanical properties of both systems progressively deteriorated with decreasing pH. At pH = 1, the P-wave velocity, peak stress, and elastic modulus of the ESCA-solidified specimens decreased by 21.7%, 72.57%, and 85.98%, respectively, compared with corresponding reductions of 42.0%, 81.07%, and 93.75% for the P.O 42.5-solidified specimens. Acid attack increased crack development and connectivity and induced a transition in failure mode from axial splitting toward mixed shear–splitting failure. SEM and CT analyses further revealed that, after immersion at pH = 1, the surface pore area fraction of the ESCA-solidified specimens increased from 8.22% to 10.44%, while the CT-derived porosity increased from 1.21% to 2.17%; both increases were lower than those observed in the P.O 42.5 system. The slower pore development and less pronounced performance degradation of the ESCA-solidified specimens indicate better preservation of the cemented structure and greater pore-structure stability, resulting in improved resistance to acid attack.

Keywords: shield muck; ESCA; acid attack; mechanical degradation; pore structure; microstructural damage

Check for updates

Academic Editor: Piotr Smarzewski

Received: 28 October 2026
Revised: 14 November 2026
Accepted: 16 November 2026
Published: 20 November 2026

Copyright: © 2026 by the authors. Licensee MDPI, Basel, Switzerland. This article is an open access article distributed under the terms and conditions of the Creative Commons Attribution (CC BY) license.

1. Introduction

With the continued development of urban underground space and infrastructure, shield tunnelling has been widely adopted in the construction of urban rail transit systems, utility tunnels, and other underground structures. However, shield excavation inevitably generates large quantities of shield muck, which is typically characterized by high water

content, complex particle composition, and limited engineering applicability. Conventional disposal practices, including off-site transportation and stockpiling, not only increase construction costs but also occupy land resources and impose additional environmental burdens. Therefore, the efficient valorization of shield muck has become an important issue in underground engineering [1]. Solidification provides an effective route for converting shield muck from a waste material into a reusable engineering material by improving its internal structure and mechanical performance through cementation [2,3].

Cement-based binders have been widely used for shield muck solidification because of their favorable hydration and bonding capacity as well as their structural stability. Hydration products can fill the pores within the soil matrix and strengthen interparticle bonding, thereby improving the strength and overall stability of the solidified material [4]. Nevertheless, conventional cement-based stabilization generally requires relatively high cement contents, while cement production is associated with substantial energy consumption and carbon emissions, which limits the broader application of this approach [5]. Accordingly, the development of more efficient and lower-carbon cementitious systems has become an important direction in solidification technology. In recent years, industrial by-products and composite mineral components have been increasingly incorporated into greener cementitious binders, in which synergistic reactions among multiple constituents regulate the formation of hydration products and improve the mechanical properties and microstructure of solidified materials [6–9]. Among these systems, calcium sulfoaluminate-based binders have attracted increasing attention because of their rapid reaction characteristics and favorable early-strength development, providing a promising route for the design of early-strength solidifying agents [10]. Multicomponent formulation also offers opportunities to balance early-age performance, material costs, and environmental impacts. Wang et al. [11] reported improved performance and cost efficiency in modified magnesium phosphate cement concrete under negative temperatures through the combined incorporation of fly ash and a small amount of early-strength Portland cement. Yoo et al. [12] reviewed cementless ultra-high-performance concrete incorporating alkali-activated materials and industrial by-products, highlighting its potential to reduce the environmental burden associated with conventional cement use. These studies provide perspectives for alternative binder development, although their benefits require verification for specific solidified-soil formulations.

Acid attack is an important environmental factor governing the long-term performance of cement-based solidified materials. Once acidic media penetrate the solidified matrix, they may react with cementitious products, resulting in decomposition of hydration products, weakening of interfacial bonding, and progressive evolution of the pore structure, ultimately leading to reductions in strength and durability. Previous studies have shown that prolonged exposure to aggressive environments can induce strength loss and internal structural degradation in cement-solidified materials [13]. Dong et al. [14] further investigated the evolution of microstructure and impermeability of cement-bound soils under acid attack and reported that acidic conditions accelerated the decomposition of cementitious products and reduced structural stability. In addition, the acid resistance of cementitious materials strongly depends on binder composition and the nature of hydration products, resulting in distinct environmental responses among different cementitious systems [15–17]. For solidified shield-derived materials, Zhang et al. [18] found that the combined effects of acid corrosion and wet–dry cycling promoted crack propagation and internal damage accumulation, leading to continuous deterioration in mechanical performance. Further studies also demonstrated that wet–dry cycling can alter the strength and deformation characteristics of solidified shield waste mud, thereby affecting its long-term service stability [19]. Zhao et al. [20] previously investigated the mechanical properties and solidification mechanism

of shield muck treated with an early-strength cementitious agent (ESCA), demonstrating favorable early-age strength and a relatively compact microstructure. Building on the same binder formulation, the present study extends the investigation to acid-exposure durability. Whether the cemented structure established during curing can withstand acidic exposure, and how its deterioration affects pore structure and mechanical performance, requires further investigation.

Accordingly, shield muck solidified with ESCA or P.O 42.5 cement was subjected to 45 d of immersion at pH values of 1, 3, 5, and 7, with unimmersed specimens providing an additional reference. Mass and P-wave velocity measurements, unconfined compression tests, SEM observations, and industrial CT analyses were combined to compare performance retention and structural changes in the two systems. The investigation examines the links between pore development, weakening of the cemented structure, and reductions in strength and stiffness, providing evidence for binder selection and durability assessment of solidified shield muck under acidic exposure.

2. Materials and Methods

2.1. Shield Muck

The shield muck used in this study was collected from the shield tunnelling project of the Jiluo Road Yellow River Crossing Tunnel in Jinan, Shandong Province, China. The sampling location is shown in Figure 1. After being transported to the laboratory, representative specimens of the shield muck were selected for physical-property testing. The water content, density, liquid and plastic limits, and compaction characteristics were determined with reference to GB/T 50123–2019 [21]. The natural water content was measured using separately retained as-received specimens. The results are summarized in Table 1. The natural water content, dry density, and optimum moisture content were 14.16%, 1.54 g/cm^3, and 14.67%, respectively, while the liquid and plastic limits were 31.25% and 18.43%, indicating the plastic characteristics of the material.

For X-ray diffraction (XRD) analysis, representative shield muck specimens were dried at 40 °C, gently ground using an agate mortar, and passed through a 75 μm sieve. The powder was back-loaded into the sample holder to reduce preferred orientation. Measurements were conducted using Cu radiation at a tube voltage of 45 kV and a tube current of 200 mA. Diffraction patterns were collected over a 2θ range of 10–90° with a step size of 0.02°. The data were analyzed using MDI Jade 9, with phase identification based on the ICDD PDF-4+ database (2009 release). Quantitative phase analysis was performed using whole-pattern fitting (WPF) and Rietveld refinement. The diffraction patterns were plotted using Origin 2024. The X-ray diffraction (XRD) results in Figure 2a show that quartz was the dominant mineral, accounting for 50.9% of the total mineral composition, followed by albite, illite, and muscovite. Overall, the mineral composition was dominated by silicate minerals. The particle-size distribution was measured by wet laser diffraction using deionized water as the dispersion medium. Representative specimens were gently disaggregated without grinding the primary particles and dispersed in the measurement medium. The suspensions were ultrasonically dispersed and continuously circulated during measurement. The particle-size distribution results (Figure 2b) showed that the characteristic particle sizes D_{10}, D_{30}, and D_{60} were 9.941, 25.44, and 44.73 μm, respectively, with a coefficient of uniformity (C_μ) of 4.50, indicating a certain degree of particle-size variation in the processed sample.

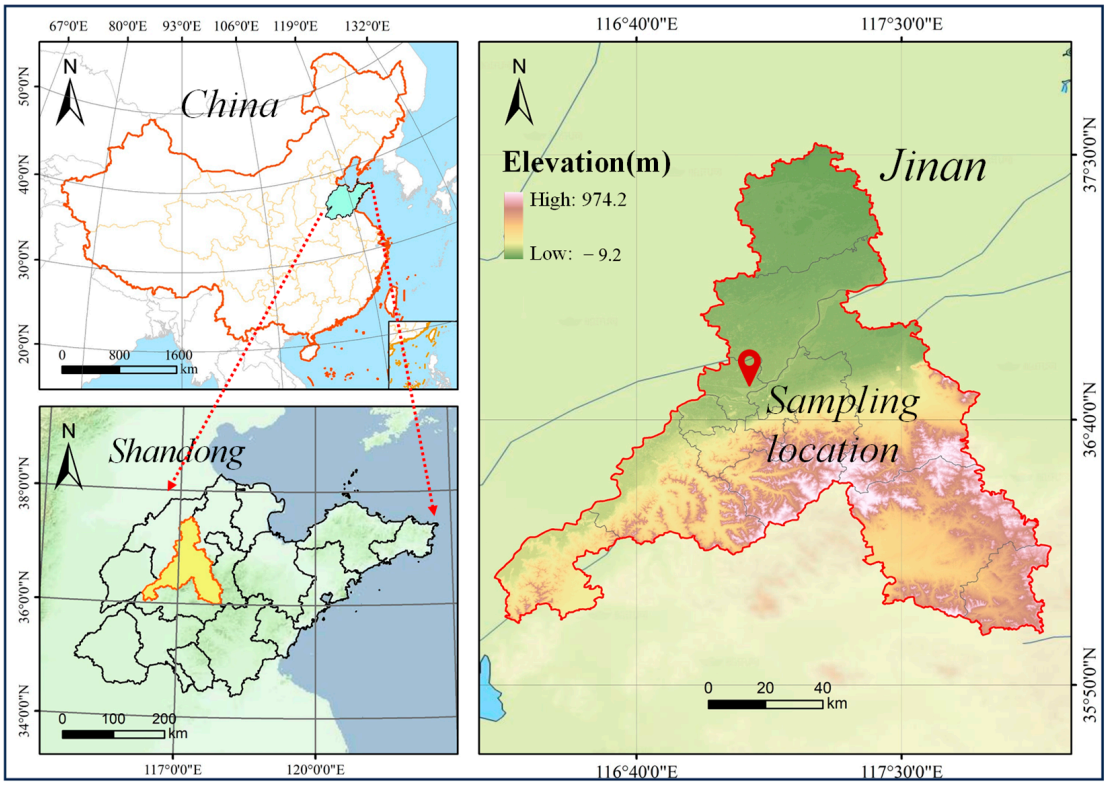


Figure 1. Location of the shield muck sampling site at the Jiluo Road Yellow River Crossing Tunnel in Jinan, China.

Table 1. Basic physical properties of the shield muck.

Physical Property	Symbol/Unit	Value
Natural water content	ω (%)	14.16
Dry density	ρ_d (g/cm^3)	1.54
Liquid limit	ω_L/%	31.25
Plastic limit	ω_P/%	18.43
Plasticity index	I_P	12.82
Optimum moisture content	ω_{opt} (%)	14.67

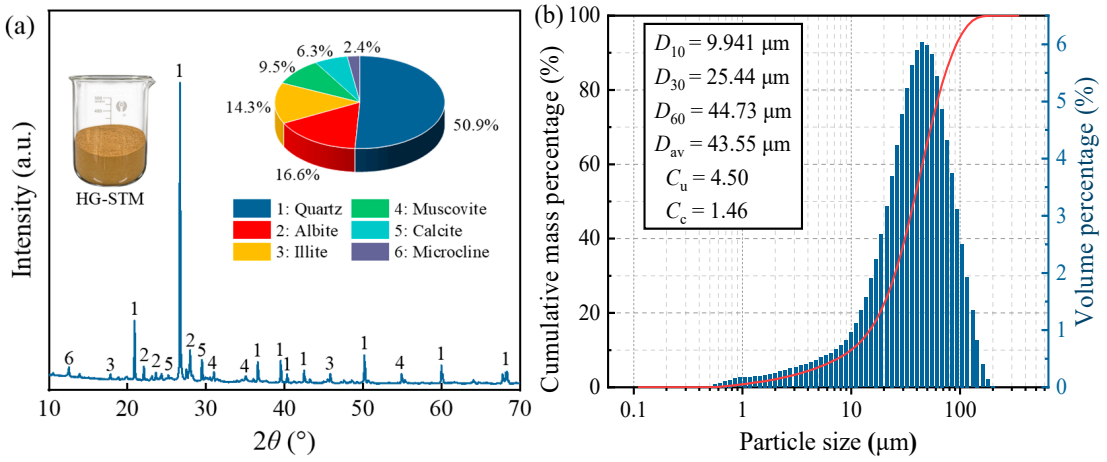


Figure 2. Mineralogical composition and particle-size distribution of the as-received shield muck: (**a**) XRD pattern and mineral composition; (**b**) particle-size distribution.

For scanning electron microscopy–energy-dispersive X-ray spectroscopy (SEM–EDS), representative shield muck specimens were dried at 40 °C, mounted on sample stubs using conductive adhesive tape, and sputter-coated with gold to reduce surface charging. SEM–EDS observations (Figure 3) revealed irregular particle morphologies with pronounced surface relief. Image analysis yielded a pore area fraction of 9.47% within the analyzed region. The EDS results in Figure 3 were obtained by area scanning and represent the local elemental composition and distribution within the scanned region, rather than an average of multiple independently selected regions. The detection of Si, Al, and O is compatible with the silicate minerals identified by XRD. However, the local EDS results are not considered representative of the bulk chemical composition of the shield muck.

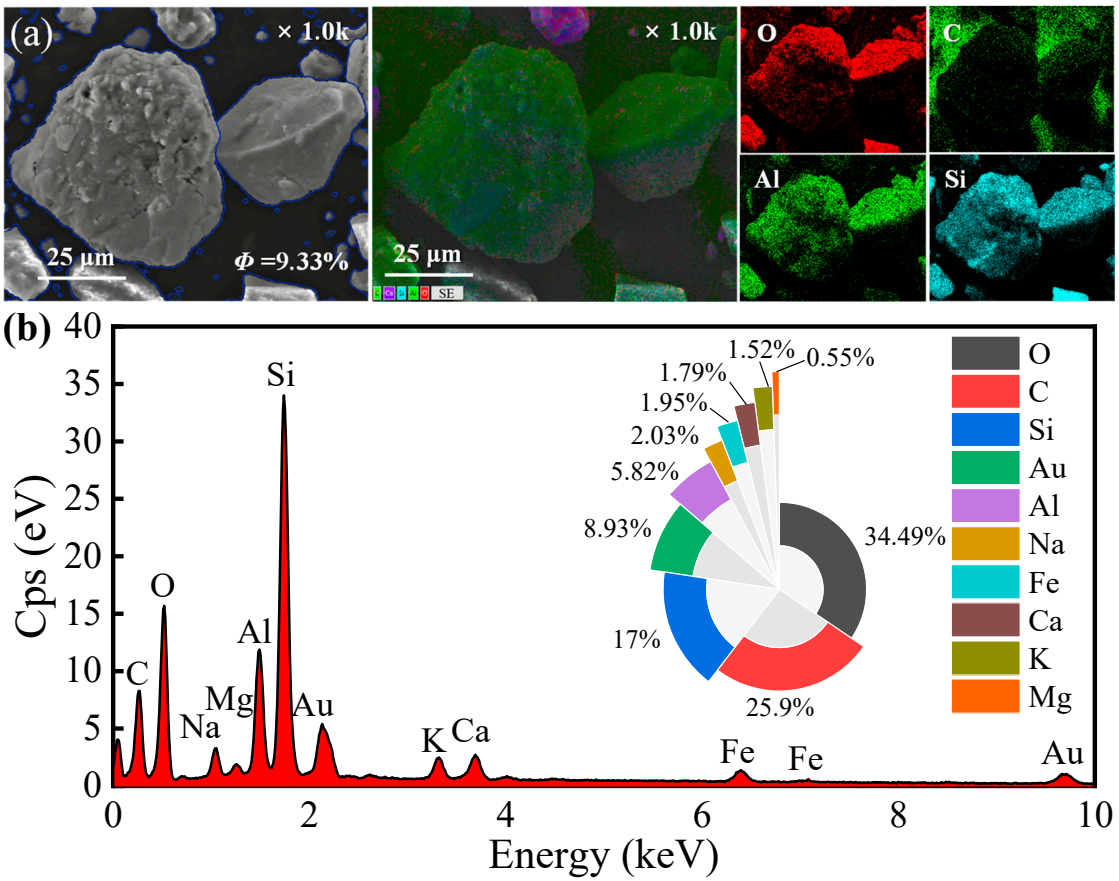


Figure 3. Local SEM–EDS characterization of the shield muck: (**a**) microstructure and elemental maps; (**b**) EDS spectrum and elemental composition obtained from the scanned area.

The pronounced carbon signal requires cautious interpretation. EDS alone cannot distinguish carbon associated with carbonate minerals, organic matter, or external sources. Mounting materials and surface contamination may contribute to the signal, but these contributions were not independently verified or quantified. Therefore, the measured carbon percentage is not used to infer bulk carbon content or quantify carbonate or organic-matter contents.

To complement the local EDS observations, the bulk major oxide composition of the shield muck was determined by X-ray fluorescence (XRF) analysis and is presented in Table 2. SiO_2 and Al_2O_3 accounted for 58.26% and 21.17%, respectively, confirming a predominantly siliceous–aluminous composition. The reported LOI of 10.60% should not be equated with organic-matter content because ignition loss can include water release, dehydroxylation, carbonate decomposition, and organic-matter combustion. The bulk oxide

composition and local EDS elemental percentages describe different quantities and are not directly interchangeable.

Table 2. Chemical compositions of shield muck, inorganic binder constituents, and P.O 42.5 cement (wt.%).

Material	CaO	SiO_2	Al_2O_3	Fe_2O_3	MgO	SO_3	Na_2O	K_2O	LOI
SAC	42.50	8.44	23.20	1.25	3.30	18.36	0.96	0.54	1.45
GGBS	41.72	33.54	14.29	0.38	5.42	2.67	0.24	0.34	1.40
FA	3.01	60.27	22.86	6.68	0.65	1.32	0.62	1.73	2.86
FGDG	30.01	2.13	0.78	0.51	1.04	44.97	0.06	0.15	20.35
P.O 42.5 cement	63.16	20.88	4.72	3.10	3.42	1.85	0.22	0.61	2.04
Shield muck	1.24	58.26	21.17	4.41	1.62	0.42	0.73	1.55	10.60

Note: LOI refers to loss on ignition. PCE is excluded from this table because it is an organic polymer admixture rather than an inorganic oxide-based constituent.

2.2. Solidifying Binders

An early-strength composite cementitious agent (ESCA) and P.O 42.5 ordinary Portland cement were used as binders for the solidification of shield muck. P.O 42.5 cement served as the conventional Portland cement reference system to evaluate the performance differences between the composite cementitious system and the conventional cement-based system under subsequent acidic exposure.

The ESCA used in this study followed the formulation reported by Zhao et al. [20]. It consisted of 45% calcium sulfoaluminate cement (SAC), 35% ground granulated blast furnace slag (GGBS), 12% fly ash (FA), 7% flue gas desulfurization gypsum (FGDG), and 1% polycarboxylate superplasticizer (PCE). The chemical compositions of the shield muck, inorganic binder constituents, and P.O 42.5 cement are presented in Table 2. SAC and FGDG favor rapid ettringite formation, contributing to early-age strength development, while GGBS and FA contribute to the development of the composite cementitious matrix. PCE promotes particle dispersion and improves mixture workability.

To evaluate the applicability of ESCA for shield muck solidification, specimens solidified with ESCA and P.O 42.5 cement were prepared and tested for compressive and tensile strengths at different curing ages. For the tests presented in Figure 4, the binder dosage was fixed at 10% for both ESCA and P.O 42.5 cement. The strength development of the two systems was therefore compared at an equal binder dosage. As shown in Figure 4, the mechanical properties of both solidification systems increased with curing age. However, the ESCA-solidified specimens exhibited consistently higher compressive and tensile strengths at 1, 7, and 28 d. The strength advantage of ESCA was particularly pronounced at early curing ages, indicating that ESCA can rapidly develop a stable cemented structure and thus provide a suitable material basis for the subsequent investigation of durability under acidic conditions.

The shield muck content is another important factor affecting the formation of the cemented structure and the resulting mechanical properties. To determine an appropriate muck content for the two solidification systems, ESCA and P.O 42.5 cement were separately used as binders, and specimens containing 50%, 60%, 70%, 80%, and 90% shield muck were prepared. Uniaxial compression tests were conducted after 28 d of curing, and the representative stress–strain curves are presented in Figure 5.

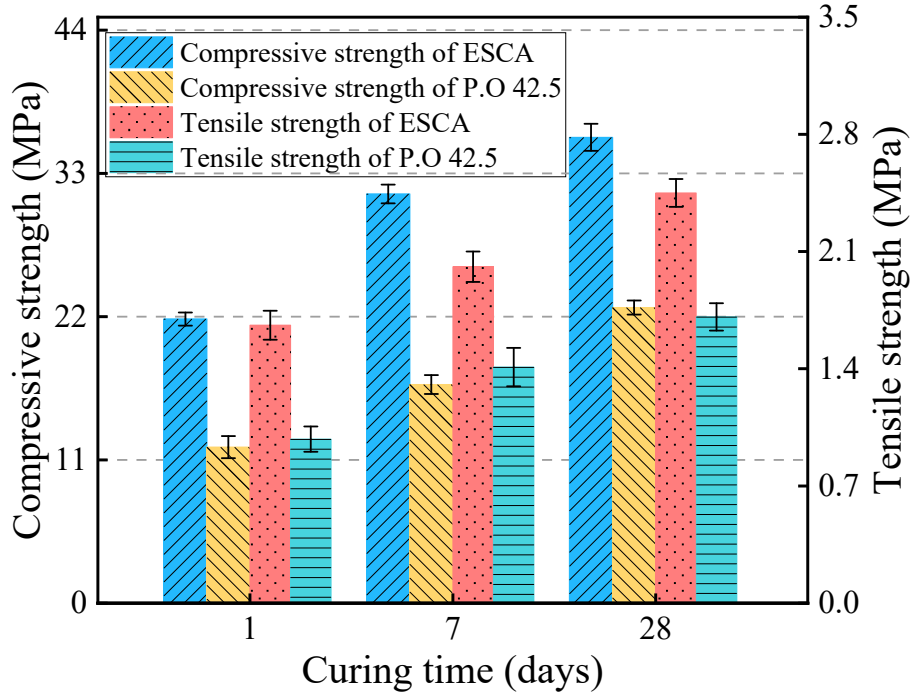
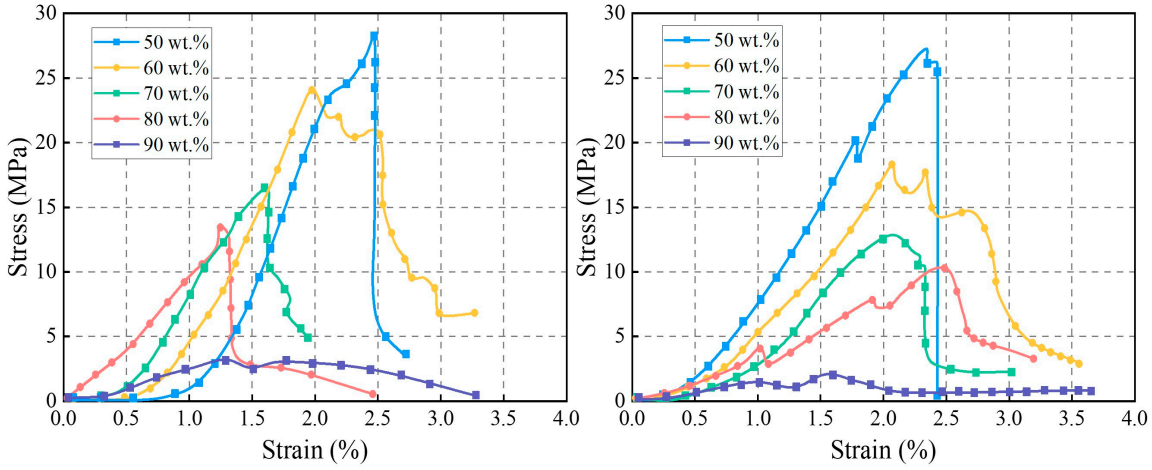


Figure 4. Compressive and tensile strengths of ESCA- and P.O 42.5-solidified shield muck at different curing ages with an equal binder dosage of 10%.



(**a**) ESCA-solidified shield muck (**b**) P.O 42.5-solidified shield muck

Figure 5. Stress–strain curves of solidified shield muck with different shield muck contents.

The peak stress of both systems decreased progressively with increasing shield muck content, indicating that a higher proportion of muck reduces the relative amount of cementitious binder and consequently weakens interparticle bonding. At the same muck content, the ESCA-solidified specimens consistently exhibited higher peak stresses and more stable post-peak deformation behavior than the P.O 42.5-solidified specimens, suggesting a greater load-bearing capacity and resistance to structural damage. Even at a shield muck content of 90%, the ESCA-solidified specimens still satisfied the strength requirement for subgrade backfill materials under heavy-traffic conditions specified in the Technical Guidelines for Construction of Highway Roadbases [22]. This result demonstrates the potential of ESCA for the high-content reuse of shield muck in engineering applications.

2.3. Experimental Methods

For the acid-resistance tests, the dry shield muck-to-binder mass ratio was fixed at 90:10 for both the ESCA and P.O 42.5 systems. Before mixing, the raw shield muck was oven-dried at 105 °C for 24 h and gently disaggregated without crushing the primary particles. Water was added at a water-to-total-dry-solids mass ratio of 0.40, where the total dry solids comprised the dry shield muck and binder. The materials were mixed for 5 min, placed into cylindrical molds in a single layer, and statically compacted under a gradually applied axial load until the prescribed specimen height was reached. A total of 30 cylindrical specimens, 50 mm in diameter and 100 mm in height, were prepared, with 15 specimens for each binder system. The specimens were protected against moisture loss before demolding and subsequently cured at 20 ± 2 °C and a relative humidity of at least 95% until an age of 28 d. After curing, the specimens were assigned to the exposure groups described below, as illustrated in Figure 6.



(**a**) Preparation of immersion solutions (**b**) Specimens during immersion

Figure 6. Immersion test procedure under different pH conditions.

Before the immersion tests, the specimens were randomly divided into five groups, each containing three specimens from each solidification system. One group remained unimmersed under natural curing conditions, while the other four groups were immersed for 45 d in solutions with pH values of 1, 3, 5, and 7. The unimmersed group provided a performance reference without immersion, whereas the pH = 7 group provided a near-neutral water-immersion reference. Comparisons with the unimmersed group characterize performance differences associated with the respective exposure histories, while comparisons between the acidic immersion groups and the pH = 7 group help assess the additional deterioration associated with lower-pH exposure. The two reference groups therefore serve different purposes and are not interchangeable. During immersion, the solutions were replaced every 9 d.

The acidity of the immersion solutions was adjusted using hydrochloric acid. By imposing different pH conditions, the effects of environmental acidity on the structural and performance evolution of solidified shield muck were investigated, and the durability of the ESCA- and P.O 42.5-solidified systems under acid attack was comparatively evaluated.

Before and after immersion, the specimens were oven-dried at 40 ± 2 °C. Changes in surface morphology were recorded using a Leica camera, while specimen mass and P-wave velocity were measured using an electronic balance and an OLYMPUS EPOCH 600 ultrasonic flaw detector, respectively, to evaluate the macroscopic deterioration induced by acid attack. To characterize the evolution of the internal structure, unimmersed specimens and specimens exposed to pH = 1 were selected from both the ESCA- and P.O 42.5-solidified systems for industrial computed tomography (CT) scanning. Two-dimensional CT slices

were acquired using a Nikon XT H 225 ST industrial CT system at a scanning resolution of 60 μm, and the internal pore structure was reconstructed in Avizo using threshold-based image segmentation.

After CT scanning, unconfined compression tests were performed using an MTS SANS universal testing machine (MTS Systems (China) Co., Ltd., Shenzhen, China) under displacement-controlled loading at a rate of 0.5 mm/min. Representative fractured fragments were subsequently selected for scanning electron microscopy (SEM) to examine the microstructural morphology and pore characteristics. SEM images acquired at ×500 magnification were converted to grayscale and subjected to threshold segmentation in ImageJ 1.54t, with low-grayscale regions identified as pores. The surface pore area fraction, Φ, was defined as the ratio of the pore area to the total analyzed area:

$$\Phi = \frac{A_P}{A_t} \times 100\% \quad (1)$$

where A_P is the pore area identified in the binarized image and A_t is the total analyzed area. During image binarization, the segmentation results were cross-checked against the corresponding original SEM images, and a consistent analysis area was adopted for all specimens to ensure comparability among different conditions. The SEM-derived pore area fraction represents the local apparent pore area on the examined fracture surface rather than the bulk volumetric porosity. Because the SEM fragments were collected after compression testing, the results may also be influenced by loading-induced damage and fracture-surface selection. The main experimental equipment used in this study is shown in Figure 7.



Figure 7. Test instruments and equipment used in the experiment. (**a**) P-wave velocity tester; (**b**) Hydraulic testing machine; (**c**) Industrial CT system; (**d**) Scanning electron microscope (SEM).

3. Results and Analysis

3.1. Appearance Changes

Figure 8 shows the surface morphology of the two solidified shield muck specimens under different pH conditions. As the pH decreased, both types of specimens exhibited progressively more pronounced surface deterioration, characterized mainly by surface roughening, discoloration, and localized erosion. The most severe surface damage occurred

at pH = 1, indicating that increasing acidity aggravated the macroscopic deterioration of the solidified material. Similar surface erosion and cracking have been reported for cementitious materials exposed to low-pH environments [23]. In comparison, the ESCA-solidified specimens maintained better surface integrity across the tested pH conditions. Combined with the subsequent SEM and CT observations, this behavior may be associated with better preservation of the cemented structure and greater pore-structure stability in the ESCA system.

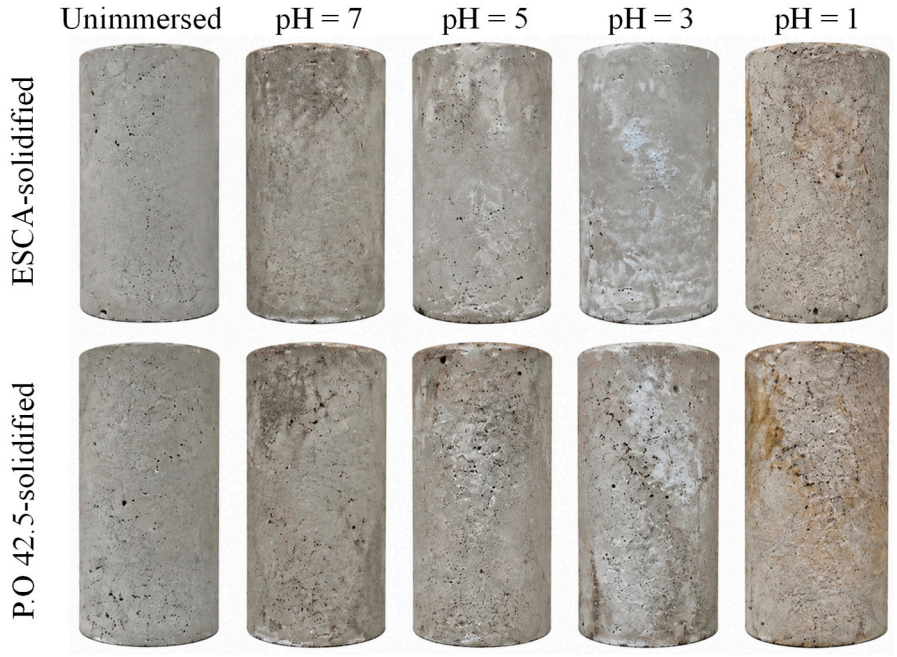


Figure 8. Appearance of ESCA- and P.O 42.5-solidified shield muck under unimmersed conditions and after 45 d of immersion in solutions with different pH values.

3.2. Changes in Mass and P-Wave Velocity

Figure 9 shows the changes in mass and P-wave velocity of the ESCA- and P.O 42.5-solidified shield muck specimens under different pH conditions, with the error bars representing standard deviations. As the pH decreased, both mass and P-wave velocity continuously decreased in the two systems. The reduction in P-wave velocity was substantially greater than the mass loss, indicating that P-wave velocity was more sensitive to acid-induced internal structural changes. Lafhaj et al. [24] found that the ultrasonic velocity of chemically damaged mortar decreased with increasing porosity. Miturski et al. [25] further demonstrated a relationship between ultrasonic response and the mechanical characteristics of cement-stabilized soil. Accordingly, the continuous reduction in P-wave velocity observed here can be regarded as a macroscopic response to progressive internal structural deterioration.

After 45 d of immersion at pH = 1, the mass and P-wave velocity of the ESCA-solidified specimens decreased by approximately 2.2% and 21.7%, respectively, compared with approximately 3.2% and 42.0% for the P.O 42.5-solidified specimens. The greater reductions in the P.O 42.5 system indicate more severe structural deterioration under strongly acidic conditions. Combined with the SEM and CT results, the smaller reduction in P-wave velocity for the ESCA system may be associated with better preservation of the cemented structure and more limited pore development.

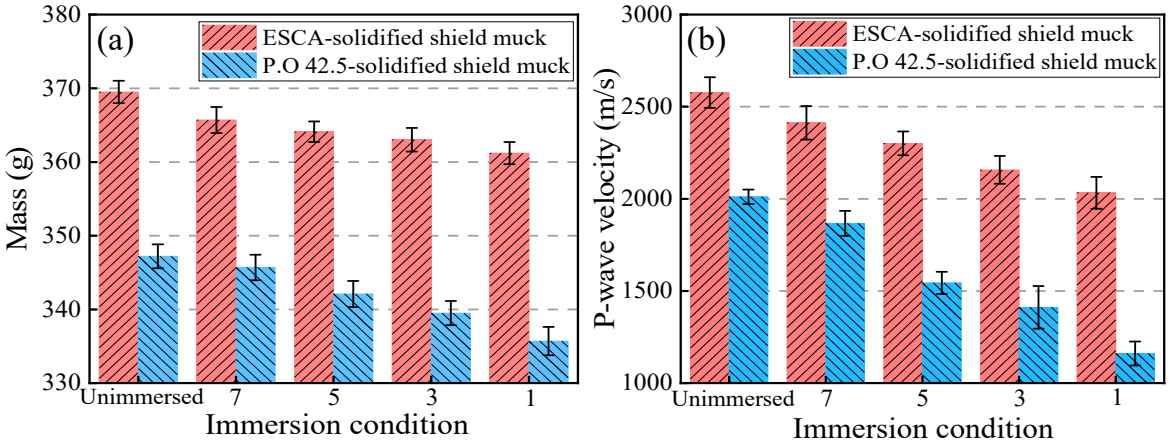


Figure 9. Mass and P-wave velocity of solidified shield muck under unimmersed conditions and after 45 d of immersion in solutions with different pH values: (**a**) mass; (**b**) P-wave velocity.

3.3. Changes in Mechanical Behavior

Figure 10 presents the stress–strain responses of the two solidified shield muck systems under different pH conditions. As the pH decreased, the peak stress of both systems progressively decreased, while the peak strain generally shifted toward higher strain levels and the stress–strain curves became flatter. These changes indicate that acid attack reduced the load-bearing capacity of the specimens while increasing their deformation response.

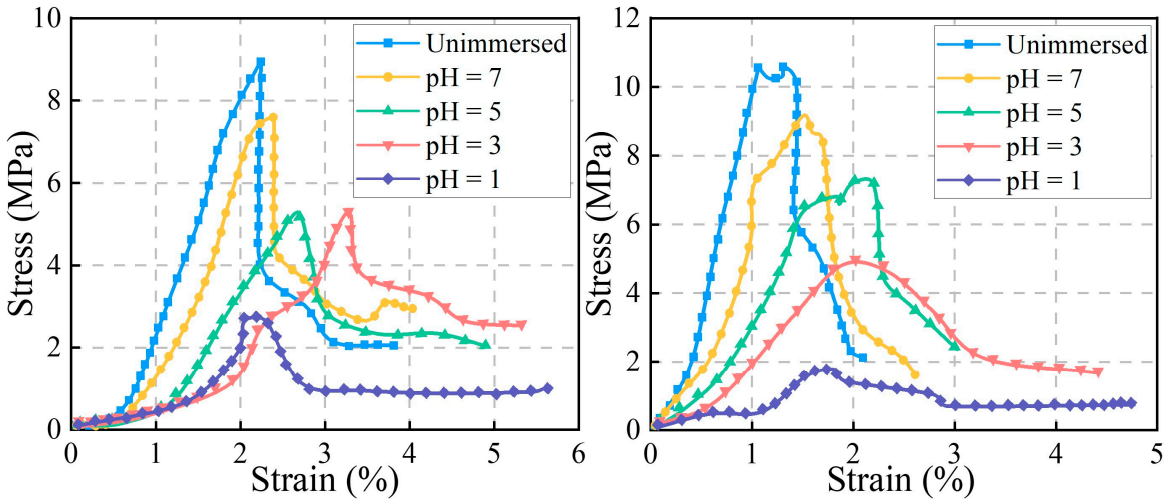


Figure 10. Stress–strain responses of solidified shield muck under unimmersed conditions and after 45 d of immersion in solutions with different pH values.

Clear differences were also observed in the post-peak behavior of the two systems. The ESCA-solidified specimens exhibited a relatively gradual post-peak stress reduction and retained a certain residual load-bearing capacity at large axial strains. In contrast, the P.O 42.5-solidified specimens showed a more pronounced post-peak stress drop at lower pH values. With increasing acidity, both systems gradually shifted from a high-strength response with a relatively distinct peak toward a lower-strength and higher-deformation response, reflecting the progressive accumulation of internal damage. Ghasemi et al. [26] similarly reported acid-induced performance degradation in cementitious materials and found strong correlations among different performance-loss indicators. Combined with the subsequent SEM and CT observations, the mechanical response observed here may be

associated with pore enlargement, reduced continuity of the cemented structure, and the development of localized defects. Overall, the ESCA system exhibited milder post-peak softening and greater residual load-bearing capacity under acid attack.

3.4. Evolution of Mechanical Parameters

Figure 11 shows the evolution of peak stress and elastic modulus of the two solidified shield muck systems under different pH conditions, with the error bars representing standard deviations. Both peak stress and elastic modulus continuously decreased with decreasing pH, demonstrating that acid attack substantially weakened the load-bearing capacity and stiffness of the specimens. The elastic modulus generally decreased more markedly than the peak stress, suggesting that stiffness was more sensitive to acid-induced structural damage.

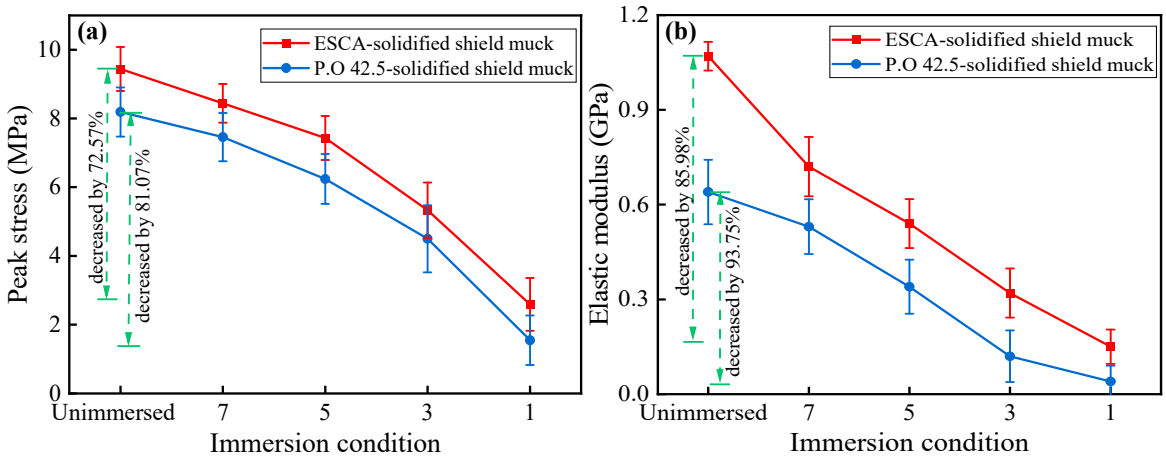


Figure 11. Mechanical properties of solidified shield muck under unimmersed conditions and after 45 d of immersion in solutions with different pH values: (**a**) peak stress; (**b**) elastic modulus.

After 45 d of immersion at pH = 1, the peak stress and elastic modulus of the ESCA-solidified specimens decreased by 72.57% and 85.98%, respectively, corresponding to retention ratios of 27.43% and 14.02%. For the P.O 42.5-solidified specimens, the corresponding reductions reached 81.07% and 93.75%, with retention ratios of only 18.93% and 6.25%. The ESCA system therefore retained a greater proportion of its strength and stiffness under strongly acidic conditions. Ukrainczyk et al. [27] also observed markedly different acid degradation responses among different binder systems, including differences in mass loss, hardness reduction, and porosity evolution, highlighting the important role of binder composition in acid resistance.

The concurrent reductions in peak stress and elastic modulus indicate that acid attack impaired both the load-bearing capacity and deformation resistance of the specimens. The greater reduction in elastic modulus further suggests that stiffness-related parameters are more sensitive to structural deterioration. The pronounced mechanical deterioration despite limited mass loss can be explained by the different structural sensitivities of these indicators. Mass loss measures the net amount of material removed from the specimen, whereas compressive strength and elastic modulus depend strongly on the integrity of cemented contacts and load-transfer paths. Acid-induced dissolution of cementitious phases can weaken interparticle bonding [27]. Localized damage to these contacts may therefore substantially reduce strength and stiffness while much of the mineral framework remains within the specimen. Furthermore, interfacial debonding and defect development can impair load transfer without causing immediate material detachment. The greater reduction in elastic modulus is consistent with increased deformation associated with

weakened contacts and internal defects. The P-wave velocity reductions and the SEM and CT observations provide complementary evidence of structural deterioration. However, selective bond damage remains a mechanistic interpretation rather than a process quantified directly in this study. Consequently, mass loss alone is insufficient to characterize the mechanical damage of solidified shield muck. Differences relative to the unimmersed group may include the effects of water immersion and differences in curing history and should therefore not be attributed exclusively to chemical acid attack. The pH = 7 group provides a near-neutral immersion reference for interpreting the additional deterioration associated with lower-pH exposure.

3.5. Failure Modes

Figures 12 and 13 show the failure patterns and crack propagation characteristics of the solidified shield muck specimens under different pH conditions. Under the unimmersed condition, both types of specimens were dominated by axial splitting, with the major cracks propagating primarily along the specimen axis. As the acidity increased, the crack patterns became progressively more complex, with increasing numbers of branch and secondary cracks accompanied by localized surface spalling.

At pH = 3 and pH = 1, the cracks exhibited greater tortuosity and more extensive branching, together with more pronounced localized damage. In particular, multidirectional crack propagation and block spalling became more evident at pH = 1, indicating that strong acid attack substantially altered the crack propagation paths and failure modes of the solidified shield muck.

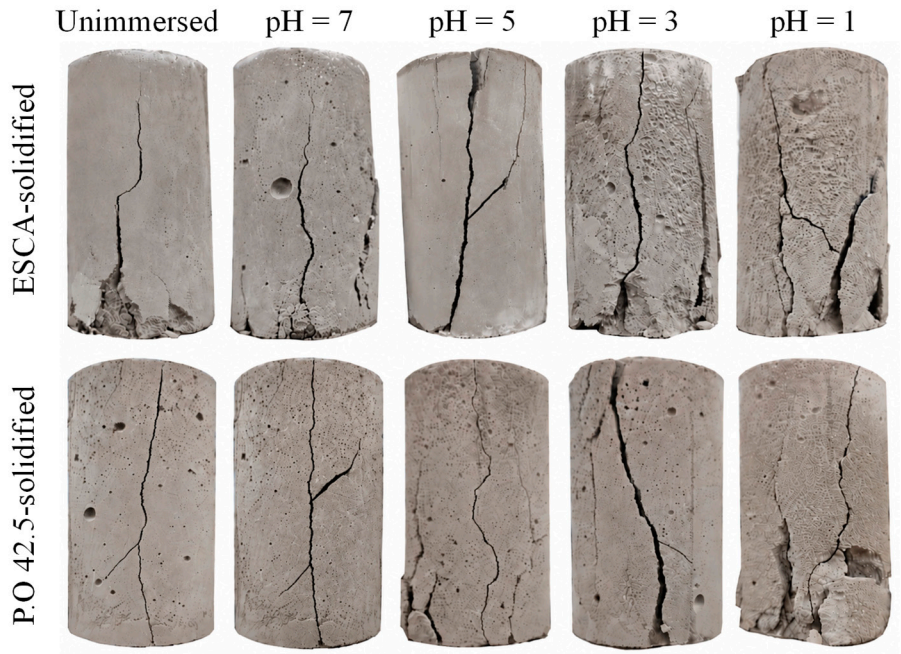


Figure 12. Failure modes of ESCA- and P.O 42.5-solidified shield muck under unimmersed conditions and after 45 d of immersion in solutions with different pH values.

The failure cracks in Figures 12 and 13 were observed after compression testing and therefore reflect the mechanical response of previously conditioned specimens, rather than cracking caused solely by immersion. Acid-induced dissolution of cementitious phases and weakening of particle–binder interfaces provide a plausible explanation for the observed changes [17,27]. The resulting weak contacts and enlarged defects can promote stress concentration and crack coalescence during subsequent loading, producing more branched cracks and mixed shear–splitting failure. Lower solution pH increases the chemical driving force for deterioration,

while the proximate cause of load-induced cracking is the weakened cemented structure. Because expansion and post-exposure phase evolution were not measured, expansive-product formation cannot be established as the principal cracking mechanism.

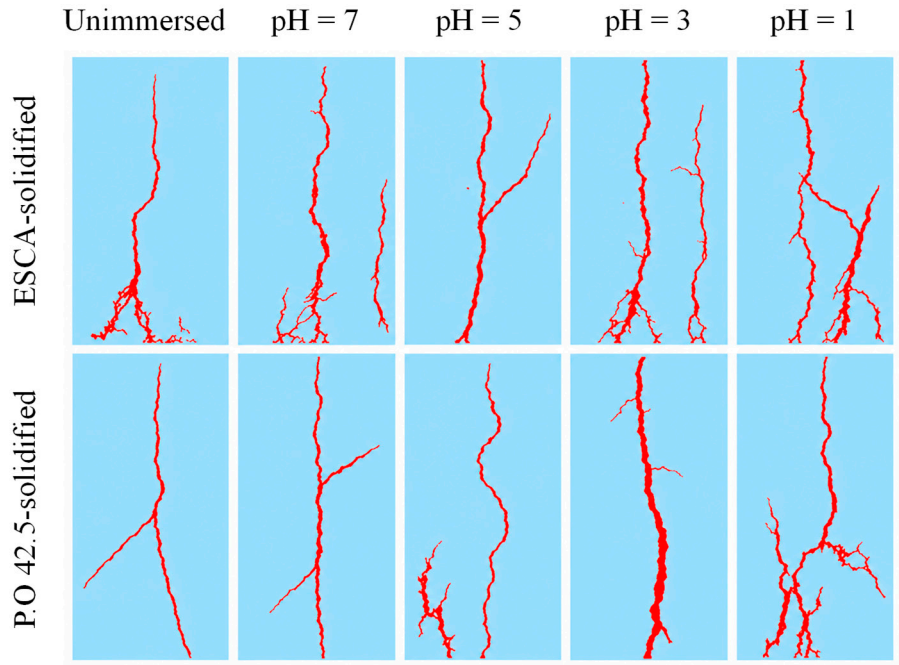


Figure 13. Extracted crack patterns of ESCA- and P.O 42.5-solidified shield muck under unimmersed conditions and after 45 d of immersion in solutions with different pH values.

3.6. SEM and CT Analyses

Figures 14 and 15 present the SEM micrographs and binarized surface-pore distributions of the two solidified shield muck systems before and after acid immersion. Under the unimmersed condition, the ESCA-solidified specimens exhibited relatively continuous cemented regions, fewer interparticle pores, and a denser overall microstructure. In contrast, the P.O 42.5-solidified specimens contained more open pores and locally loose regions. After immersion at pH = 1, both systems showed reduced continuity of the cemented structure, increased pore exposure, and localized structural loosening, with these changes being more pronounced in the P.O 42.5 system. Zhao et al. [28] similarly observed binder-dependent differences in acid-induced deterioration and corrosion-layer microstructure, indicating that binder composition plays an important role in microstructural stability under acid attack. The binarization results showed that the surface pore area fraction of the ESCA- and P.O 42.5-solidified specimens increased from 8.22% and 16.62% to 10.44% and 24.22%, respectively, corresponding to increases of 2.22 and 7.60 percentage points. The substantially greater increase in the P.O 42.5 system indicates more pronounced pore development.

Figure 16 shows that the CT-derived porosities, n, of the unimmersed ESCA- and P.O 42.5-solidified specimens were 1.21% and 1.22%, respectively, indicating nearly identical initial porosity levels. After 45 d of immersion at pH = 1, the porosities increased to 2.17% and 2.96%, respectively, with a greater increase observed in the P.O 42.5 system. The three-dimensional reconstructions further revealed that acid attack promoted the enlargement and interconnection of internal pores, with more severe pore-structure deterioration in the P.O 42.5 system. Similar relationships between pore-network evolution, crack propagation, and macroscopic mechanical degradation have also been reported in rock materials subjected to thermal–acid treatment, where CT and SEM analyses provided complementary evidence of multiscale structural damage [29]. The pore network has been identified as an important

structural factor governing the chemo-mechanical degradation of cementitious materials under aggressive exposure [30]. Taken together, the SEM and CT results demonstrate that the ESCA system better preserved its cemented structure and pore stability under strongly acidic conditions, providing a microstructural explanation for its smaller reductions in P-wave velocity and mechanical performance.

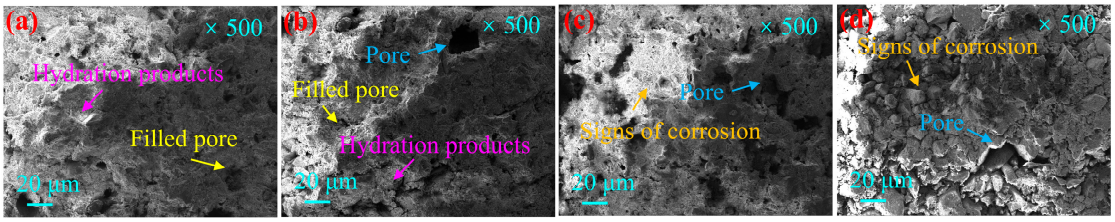


Figure 14. SEM micrographs of solidified shield muck before and after immersion at pH = 1: (**a**) unimmersed ESCA-solidified shield muck; (**b**) ESCA-solidified shield muck after immersion at pH = 1; (**c**) unimmersed P.O 42.5-solidified shield muck; (**d**) P.O 42.5-solidified shield muck after immersion at pH = 1.

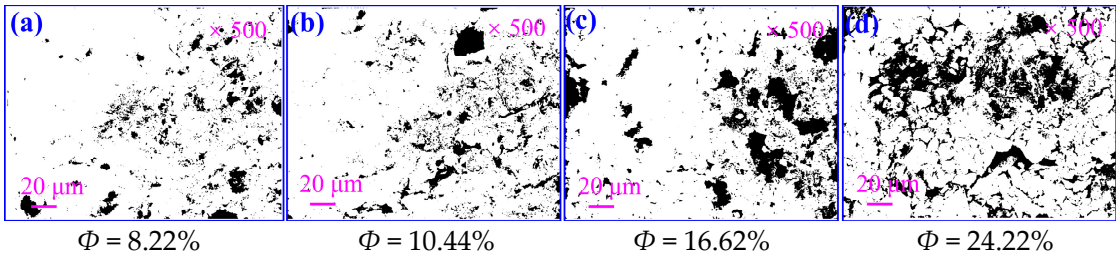


Figure 15. Surface pore distributions derived from binarized SEM images: (**a**) unimmersed ESCA-solidified shield muck; (**b**) ESCA-solidified shield muck after immersion at pH = 1; (**c**) unimmersed P.O 42.5-solidified shield muck; (**d**) P.O 42.5-solidified shield muck after immersion at pH = 1.

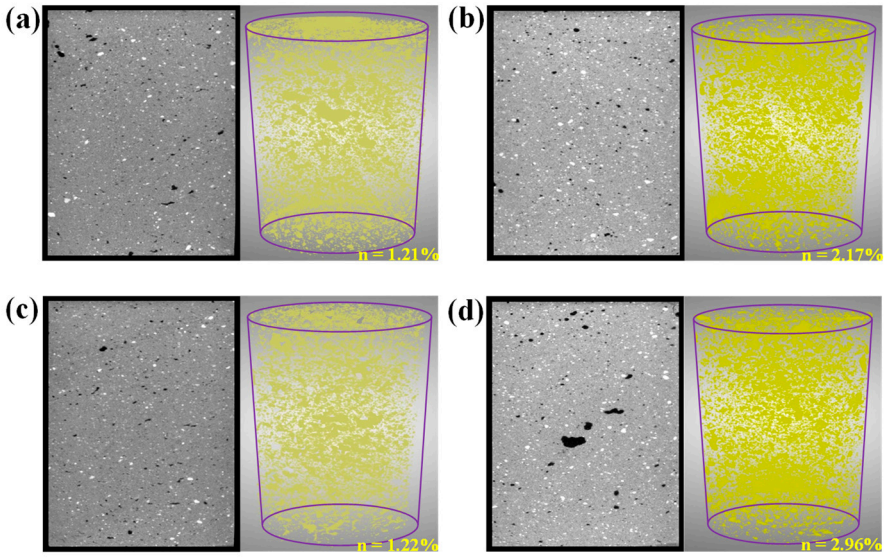


Figure 16. CT slices and 3D pore reconstructions of solidified shield muck before and after immersion at pH = 1: (**a**) unimmersed ESCA-solidified shield muck; (**b**) ESCA-solidified shield muck after immersion at pH = 1; (**c**) unimmersed P.O 42.5-solidified shield muck; (**d**) P.O 42.5-solidified shield muck after immersion at pH = 1.

The improved performance retention of ESCA cannot be attributed solely to lower initial porosity or higher initial strength. The unimmersed specimens had nearly identical CT-derived porosities of 1.21% and 1.22%, and permeability was not measured. Although the SEM images showed more continuous cemented regions in ESCA, these local fracture-surface observations do not establish lower bulk permeability. More directly, after immersion at pH = 1, CT-derived porosity increased by 0.96 percentage points for ESCA, compared with 1.74 percentage points for P.O 42.5. ESCA also retained 27.43% of its reference peak stress and 14.02% of its reference elastic modulus, compared with 18.93% and 6.25%, respectively, for P.O 42.5. These normalized results indicate that its advantage extends beyond a higher initial strength.

Together, the results support better preservation of the cemented structure and less pronounced pore development in ESCA. Binder chemistry may contribute to this response [17], but the present measurements do not isolate the contributions of individual hydrates. In particular, without post-exposure phase quantification or leachate analysis, the improved resistance cannot be assigned to greater acid stability of ettringite relative to C–S–H. The respective contributions of hydrate chemistry, unresolved fine pores, and transport properties require further investigation.

The difference between the SEM-derived pore area fraction and CT-derived porosity arises from their different measurement definitions, observation scales, and specimen states. SEM quantifies two-dimensional low-grayscale regions on selected fracture surfaces, whereas CT quantifies the segmented pore volume within a three-dimensional region of interest. At the reported CT resolution of 60 μm, smaller pores and narrow cracks may remain unresolved, and partial-volume effects and segmentation thresholds can influence the calculated pore volume. By contrast, SEM resolves finer local features, but surface relief, shadowing, particle pull-out, and compression-induced damage may affect the apparent pore area. Therefore, the SEM area fraction should not be directly equated with CT porosity. The two methods provide complementary observations: within each method, the increase in the corresponding pore index after exposure at pH = 1 was smaller for ESCA than for P.O 42.5.

The potential influence of oven drying should also be considered when interpreting the microstructural results. Drying can alter the hydration state and crystallinity of ettringite and may consequently affect the measured pore structure. Although the low drying temperature of 40 ± 2 °C was adopted to limit thermal alteration, it does not guarantee complete preservation of the hydrated phases. Moreover, applying the same drying procedure to both binder systems does not necessarily produce identical effects because their hydrate assemblages differ. The observed microstructural changes should therefore be interpreted within the adopted conditioning procedure, rather than attributed exclusively to acid attack. Further comparisons using alternative drying procedures would help distinguish acid-induced damage from drying-related changes.

The acid-resistance comparison should be distinguished from environmental and economic assessment. Lower-calcium by-product binders may reduce the availability of acid-susceptible calcium-bearing phases, but their performance also depends on hydrate chemistry, pore structure, and the exposure medium [27,28]. The present study did not quantify the carbon footprints or costs of ESCA and P.O 42.5. Consequently, the higher performance retention of ESCA under the tested conditions does not establish lower embodied carbon or lower cost. A quantitative comparison requires verified constituent proportions and production, processing, and transport inventories under consistent system boundaries and functional units.

4. Conclusions

This study systematically compared the macroscopic performance, failure behavior, and microstructural evolution of ESCA- and P.O 42.5-solidified shield muck under different pH immersion conditions. The main conclusions are as follows:

(1) Acid attack caused progressive deterioration in the physical properties of both solidification systems, and the extent of degradation increased with decreasing pH. After 45 d of immersion at pH = 1, the mass and P-wave velocity of the ESCA-solidified specimens decreased by approximately 2.2% and 21.7%, respectively, whereas those of the P.O 42.5-solidified specimens decreased by approximately 3.2% and 42.0%. These results indicate that the ESCA system maintained greater structural stability under strongly acidic conditions.

(2) The peak stress and elastic modulus of both solidification systems decreased markedly with increasing acidity, while the ESCA-solidified specimens exhibited higher retention of mechanical performance. At pH = 1, the peak stress and elastic modulus of the ESCA-solidified specimens decreased by 72.57% and 85.98%, respectively, compared with reductions of 81.07% and 93.75% for the P.O 42.5 system. In addition, the ESCA-solidified specimens exhibited a more gradual post-peak softening response, indicating greater resistance to structural damage.

(3) After acidic conditioning, the compression-induced failure pattern shifted from predominantly axial splitting toward mixed shear–splitting failure at pH $\leq$ 3. The increased crack branching is consistent with weakened cemented contacts and enlarged defects that facilitate crack coalescence during loading. The results support dissolution-related structural weakening as a plausible mechanism, whereas expansion-induced damage was not established.

(4) ESCA exhibited smaller increases in the SEM-derived pore area fraction and CT-derived porosity, together with higher relative strength and stiffness retention. Despite nearly identical initial CT-derived porosities, its CT porosity increased by 0.96 percentage points after immersion at pH = 1, compared with 1.74 percentage points for P.O 42.5. These results associate its improved acid resistance with better preservation of the cemented structure. The contributions of permeability and individual hydrate stability remain unresolved.

Author Contributions: L.Z.: Conceptualization, supervision, writing—review and editing. L.M.: Investigation, software, formal analysis, visualization, writing—review and editing. J.L. (Jie Li): Supervision, visualization. F.C.: Validation, software, project administration. H.Z.: Conceptualization, project administration, supervision, validation, writing—review and editing; S.Z.: Investigation, methodology, formal analysis, writing—original draft; J.L. (Jin Li): Software, formal analysis, visualization, validation; J.B.: Formal analysis, conceptualization, supervision, writing—review and editing. B.G.: Validation, writing—original draft, methodology. F.J.: Formal analysis, writing—review and editing. All authors have read and agreed to the published version of the manuscript.

Funding: This study was financially supported by the Key R&D Program of Shandong Province, China (Grant No. 2026CXPT181), the National Natural Science Foundation of China (Grant Nos. 52608754 and 52478460), and the Shandong Provincial Natural Science Foundation (Grant Nos. ZR2024ME054, ZR2025LH142, ZR2024QE495, and ZR2026QC0469).

Data Availability Statement: The original contributions presented in this study are included in the article. Further inquiries can be directed to the corresponding authors.

Conflicts of Interest: Authors Jie Li and Fengming Chu were employed by Tai'an Xiaoran Landscape and Municipal Engineering Co., Ltd. The remaining authors declare that the research was conducted in the absence of any commercial or financial relationships that could be construed as a potential conflict of interest.

References

1. Wu, Z.; Ye, C.; Cao, F. Performance and Microstructure of Grouting Materials Made from Shield Muck. *Materials* **2024**, *17*, 4074. [CrossRef]
2. Jiao, N.; Ding, J.; Wan, X.; Gao, M.; Xue, C. Mechanical Properties and Micro-Mechanism of Improved Shield Tunnel Muck with Phosphogypsum and Lime. *Constr. Build. Mater.* **2024**, *411*, 134437. [CrossRef]
3. Jiao, N.; Wan, X.; Ding, J.; Zhang, X.; Xue, C. Mechanical properties and microstructure of lime-treated shield tunnel muck improved with carbide slag and soda residue. *Constr. Build. Mater.* **2024**, *428*, 136419. [CrossRef]
4. Liu, L.; Deng, T.; Deng, Y.; Zhan, L.; Horpibulsuk, S.; Wang, Q. Stabilization nature and unified strength characterization for cement-based stabilized soils. *Constr. Build. Mater.* **2022**, *336*, 127544. [CrossRef]
5. Mohammed, A.A.; Nahazanan, H.; Nasir, N.A.M.; Huseien, G.F.; Saad, A.H. Calcium-based binders in concrete or soil stabilization: Challenges, problems, and calcined clay as partial replacement to produce low-carbon cement. *Materials* **2023**, *16*, 2020. [CrossRef]
6. Wei, M.; Yang, Y.; Xiong, L.; Wu, W.; Feng, T.; Zhong, K. Cement-SG curing agent for solidification of mucky soils. *Bull. Eng. Geol. Environ.* **2023**, *82*, 236. [CrossRef]
7. Ren, Z.; Wang, L.; Wang, H.; Liu, S.; Liu, M. Solidification/stabilization of lead-contaminated soils by phosphogypsum slag-based cementitious materials. *Sci. Total Environ.* **2023**, *857*, 159552. [CrossRef]
8. Huang, Q.; Yang, G.; Li, C.; Guo, M.; Wang, T.; Jiang, L. Use of alkali-activated slag as an environment-friendly agent for high-performance stabilized soil. *Materials* **2023**, *16*, 4803. [CrossRef]
9. Zhang, H.; Liu, T.; Wang, W.; Cui, Y.; Wu, Y.; Qiu, X. Effective curing of waste mud from slurry shield tunnels using OPC-MCA: Experimental investigations and microstructural analysis. *Tunn. Undergr. Space Technol.* **2025**, *161*, 106554. [CrossRef]
10. Sun, Z.; Nie, S.; Zhou, J.; Li, H.; Chen, Z.; Xu, M.; Mu, R.; Wang, Y. Hydration mechanism of calcium sulfoaluminate-activated supersulfated cement. *J. Clean. Prod.* **2022**, *333*, 130094. [CrossRef]
11. Wang, Q.; Huang, X.; Xu, S.; Wang, F. Mechanical performance and hydration characteristics of modified magnesium phosphate cement concrete under negative temperatures. *Constr. Build. Mater.* **2025**, *493*, 143186. [CrossRef]
12. Yoo, D.-Y.; Banthia, N.; You, I.; Lee, S.-J. Recent advances in cementless ultra-high-performance concrete using alkali-activated materials and industrial byproducts: A review. *Cem. Concr. Compos.* **2024**, *148*, 105470. [CrossRef]
13. Wang, P.; Chen, X.; Zeng, G.; Dong, Z.; Liu, S.; Zhang, X.; Wang, C. Long-Term Performance of Cement-Stabilized/Solidified Pb-Contaminated Soil under Simulated Erosive Environments. *Water* **2022**, *14*, 3314. [CrossRef]
14. Dong, Z.; Wan, Y.; Wang, P.; Chen, Z.; He, X.; Hui, X. Effect of long-term acid attack on impermeability and microstructure of compacted cement-bound soils. *Environ. Technol.* **2023**, *44*, 4371–4379. [CrossRef]
15. Damion, T.; Chaunsali, P. Evaluating acid resistance of Portland cement, calcium aluminate cement, and calcium sulfoaluminate based cement using acid neutralisation. *Cem. Concr. Res.* **2022**, *162*, 107000. [CrossRef]
16. Damion, T.; Cepuritis, R.; Chaunsali, P. Sulfuric acid and citric acid attack of calcium sulfoaluminate-based binders. *Cem. Concr. Compos.* **2022**, *130*, 104524. [CrossRef]
17. Huo, G.; Jiang, X.; Sun, X.; Li, H.; Shi, H. Performance of high-belite calcium sulfoaluminate cement subjected to hydrochloric acid and sulfuric acid. *Front. Mater.* **2024**, *10*, 1282919. [CrossRef]
18. Zhang, H.; Liu, T.; Cui, Y.; Wang, W.; Qing, C. Experimental study on the performance of basalt fiber combined with cement-based material solidified shield waste mud under the coupled effects of acid corrosion and dry-wet cycles. *Constr. Build. Mater.* **2025**, *463*, 140110. [CrossRef]
19. Zhang, H.; Liu, T.; Cui, Y.; Wang, Z.; Wang, W.; Zheng, J. Compression and shear properties of OPC-MCA and basalt fiber cured shield waste mud after dry-wet cycles. *Constr. Build. Mater.* **2024**, *426*, 136153. [CrossRef]
20. Zhao, L.; Zhang, H.; Yu, X.; Zhao, X.; Chen, J. Mechanical Properties and Microscopic Mechanism of Shield Tunnel Spoil Stabilized with ESCA. *Materials* **2026**, *19*, 2345. [CrossRef]
21. *GB/T 50123–2019*; Standard for Geotechnical Testing Method. Ministry of Housing and Urban-Rural Development of the People's Republic of China; State Administration for Market Regulation; China Planning Press: Beijing, China, 2019.
22. *JTG/T F20-2015*; Technical Guidelines for Construction of Highway Roadbases. Research Institute of Highway, Ministry of Transport; China Communications Press: Beijing, China, 2015.
23. Oliwa, K.; Kozub, B.; Łoś, K.; Łoś, P.; Korniejenko, K. Assessment of Durability and Degradation Resistance of Geopolymer Composites in Water Environments. *Materials* **2025**, *18*, 3892. [CrossRef]
24. Lafhaj, Z.; Goueygou, M.; Djerbi, A.; Kaczmarek, M. Experimental study on sound and damaged mortar: Variation of ultrasonic parameters with porosity. *Constr. Build. Mater.* **2009**, *23*, 953–958. [CrossRef]
25. Miturski, M.; Sas, W.; Radzevičius, A.; Šadzevičius, R.; Skominas, R.; Stelmaszczyk, M.; Głuchowski, A. Effect of Dispersed Reinforcement on Ultrasonic Pulse Velocity in Stabilized Soil. *Materials* **2021**, *14*, 6951. [CrossRef]
26. Ghasemi, A.; Soleimani Amiri, S.; Mirvalad, S.; Habibnejad Korayem, A. Evaluation of the phase composition, microstructure, mechanical performance, and resistance to acid attack of blended cement paste composed of binary trass-cement system. *Constr. Build. Mater.* **2022**, *333*, 127356. [CrossRef]

27. Ukrainczyk, N.; Muthu, M.; Vogt, O.; Koenders, E. Geopolymer, Calcium Aluminate, and Portland Cement-Based Mortars: Comparing Degradation Using Acetic Acid. *Materials* **2019**, *12*, 3115. [CrossRef]
28. Zhao, W.; Fan, Z.; Li, X.; Kong, L.; Zhang, L. Characterization and Comparison of Corrosion Layer Microstructure between Cement Mortar and Alkali-Activated Fly Ash/Slag Mortar Exposed to Sulfuric Acid and Acetic Acid. *Materials* **2022**, *15*, 1527. [CrossRef]
29. Zhang, H.; Liu, T.; Wang, W.; Cui, Y.; Zhang, D. Experimental study on multiscale damage mechanism of diorite under the effects of high temperature and acidic environment. *Rock Mech. Rock Eng.* **2026**, *59*, 6145–6168. [CrossRef]
30. Neji, M.; Dewitte, C.; Durville, B. Influence of porosity network on the chemo-mechanical evolution of low-pH cementitious materials subjected to calcareous attack. *Constr. Build. Mater.* **2023**, *405*, 133313. [CrossRef]

Disclaimer/Publisher's Note: The statements, opinions and data contained in all publications are solely those of the individual author(s) and contributor(s) and not of MDPI and/or the editor(s). MDPI and/or the editor(s) disclaim responsibility for any injury to people or property resulting from any ideas, methods, instructions or products referred to in the content.